HHS Public Access

Author manuscript

Dev Cell. Author manuscript; available in PMC 2016 May 26.

Published in final edited form as:

Dev Cell. 2015 May 26; 33(4): 388–400. doi:10.1016/j.devcel.2015.03.010.

Sarcomeres pattern proprioceptive sensory dendritic endings through Perlecan/UNC-52 in *C. elegans*

Xing Liang[1,2], **Xintong Dong**[3], **Donald G. Moerman**[4], **Kang Shen**[1,3,5], and **Xiangming Wang**[1,5]

[1]National Laboratory of Biomacromolecules, Institute of Biophysics, Chinese Academy of Sciences, 15 Datun Road, Chaoyang District, Beijing 100101, China.

[2]University of Chinese Academy of Sciences, Beijing 100101, China.

[3]Howard Hughes Medical Institute, Department of Biology, Stanford University, Stanford, California, 94305-5020, USA.

[4]Department of Zoology, University of British Columbia, Vancouver, B.C., V6T 1Z3, Canada.

Abstract

Sensory dendrites innervate peripheral tissues through cell-cell interactions that are poorly understood. The proprioceptive neuron PVD in *C. elegans* extends regular terminal dendritic branches between muscle and hypodermis. We found that the PVD branch pattern was instructed by adhesion molecule SAX-7/L1CAM, which formed regularly spaced stripes on the hypodermal cell. The regularity of the SAX-7 pattern originated from the repeated and regularly spaced dense body of the sarcomeres in the muscle. The extracellular proteoglycan, UNC-52/Perlecan, links the dense body to the hemidesmosome on the hypodermal cells, which in turn instructed the SAX-7 stripes and PVD dendrites. Both UNC-52 and hemidesmosome components exhibited highly regular stripes that interdigitated with the SAX-7 stripe and PVD dendrites, reflecting the striking precision of subcellular patterning between muscle, hypodermis and dendrites. Hence, the muscular contractile apparatus provides the instructive cues to pattern proprioceptive dendrites.

Keywords

Sarcomere; UNC-52; SAX-7; PVD; Proprioceptive dendrite

Introduction

Dendrite morphogenesis is a critical step to establish the receptor fields of neurons and to assembly functional neural circuits (Arikkath, 2012). Dendrites exhibit highly branched morphology, which suggests that dendrite development might require distinct molecular

[5]Correspondence authors: kangshen@stanford.edu, xmwang@moon.ibp.ac.cn.

programs compared to its axonal counterpart (Jan and Jan, 2010). Most of our understanding of the molecular mechanisms regulating dendritic branching comes from studies of the dendritic arborization neurons in *Drosophila melanogaster* (Corty et al., 2009; Jan and Jan, 2010). From studies in hippocampal and cortical neurons several classes of molecules that control dendritic arborization have been isolated (Arikkath, 2012). Both extrinsic and intrinsic factors including secreted proteins, cell surface receptors, cell adhesion molecules, signaling molecules, regulators of the actin cytoskeleton, and transcription factors are implicated in various aspects of dendrite development.

In the vertebrate somatosensory system, sensory nerve terminals interact with specialized non-neuronal cell types to form peripheral sensory organs. For example, the Merkel cell associated with the sensory fibers to form a gentle touch receptor. While the Merkel cell is required for generating specific touch sensation, the developmental mechanism for the association between the neurites and the Merkel cells is not understood (Ikeda et al., 2014; Woo et al., 2014). In the vertebrate proprioceptive system, sensory terminals wrap around specialized muscle fibers to form the encapsulated sensory receptors: the muscle spindles (Bewick and Banks, 2014). Little is known about the cell-cell interactions during the development of this sensory receptor.

Interactions between dendrites and the environment are important for dendrite morphogenesis. For sensory dendrites, the extracellular matrix (ECM) constitutes the growing substrates for dendrite development and often contains instructive cues. For example, the *Drosophila* class IV dendritic arborization (da) neurons grow their dendrites mainly in a 2D space on the extracellular matrix (ECM) secreted by the epidermis. The integrin-ECM interaction controls dendrite positioning on or within the epidermis by promoting dendritic retention on the basal surface (Han et al., 2012; Kim et al., 2012). The matrix metalloproteinase (Mmp) is required for the *Drosophila* sensory neurons dendrite reshaping through local degradation of the basement membrane upon which dendrites of the sensory neurons innervate (Yasunaga et al., 2010). In zebrafish, skin derived heparin sulfate proteoglycan guide peripheral sensory axon guidance to innervate the skin through the activation of the LAR receptors (Wang et al., 2012). These isolated examples represent our current understandings of the interactions between dendrite and surrounding cells during development. For proprioceptive neurons, little is known about how the muscle spindle forms.

The *C. elegans* PVD and FLP neurons are the only highly branched neurons in the entire ensemble of worm neurons (Albeg et al., 2011). Both PVD and FLP neurons are mechanosensors for the body and head, respectively. PVD responds to harsh mechanical stimuli and cold temperatures (Chatzigeorgiou et al., 2010; Way and Chalfie, 1989), and may have a role in proprioception as ablation of PVD leads to defective posture (Albeg et al., 2011). PVDs are born at the L2 stage and elaborate a series of perpendicularly oriented dendritic branches at stereotyped positions. The 1° branches emerge from the cell body, while the 2°, 3° and 4° branches for the candelabra like branch units called “menorah”. The 4° branches only grow between the muscles and the hypodermal cells and are quite regular in spacing.

Previous studies have reported several molecules involved in PVD dendrite development. For example, several transcription factors control discrete steps in PVD development by promoting or limiting branching (Smith et al., 2013; Smith et al., 2010). The fusogen EFF-1 activities may act as a quality control mechanism to sculpt PVD dendritic branches (Oren-Suissa et al., 2010). The shape of menorah is likely instructed by receptor-ligand interactions between PVD and its environment. Our previous work showed that DMA-1, a trans-membrane LRR protein, is the essential receptor in PVD for patterning menorahs (Liu and Shen, 2012). DMA-1 senses hypodermal derived signals SAX-7/L1CAM and MNR-1 in a tripartite ligand-receptor complex, which spatially instructs the growth and branching of PVD dendrites (Dong et al., 2013; Salzberg et al., 2013). SAX-7 is specifically localized to the sublateral line on the hypodermal cell and this pre-patterned cue directs 3° branches growth. The developmental cues for 4° branches remain unknown.

Here we reported that the 4° branches were also guided by SAX-7, which formed regular subcellular stripes on the hypodermal cell surface, a pattern that mirrored the sarcomere pattern in the adjacent muscle cells. We found that UNC-52/Perlecan, a basement membrane protein (Rogalski et al., 1995; Rogalski et al., 1993), that links the dense body of sarcomeres to the hemidesmosome-like fibrous organelles (FOs) on the hypodermal cells, was required for the proper pattern of the 4° branch growth. We further showed that the FO associated intermediate filaments were required for the subcellular pattern of SAX-7 in the hypodermal cells and the normal PVD dendrite pattern.

Results

PVD 4° dendrites co-localize with hypodermal SAX-7 stripes

Previous studies by Bulow's group and ours showed that trans-membrane cell adhesion molecule SAX-7, together with a novel membrane protein MNR-1, function in the hypodermal cells to guide the growth and branching of the 2° and 3° branches (Dong et al., 2013; Liu and Shen, 2012; Salzberg et al., 2013). SAX-7 localized to two longitudinal stripes, which provided the growth and branching signal for PVD 3° dendrites (Fig. 1A–D). However, what patterns the PVD 4° dendrites remains unknown.

Using a spinning disk confocal microscope equipped with a highly sensitive digital camera, we found that hypodermal cell expressed SAX-7::YFP also localized to dense parallel stripes between the muscle cell and the hypodermis, where PVD elaborated its quaternary dendritic branches (Fig. 1A–C). To test if endogenous SAX-7 showed a similar distribution pattern, we stained the wild type animals with a polyclonal SAX-7 antibody (Zhou et al., 2008) and observed a very similar stripe pattern (Fig. 1E). It is worth noting that the stripes from both the transgene and the endogenous staining were only found within the muscle quadrants. Strikingly, all PVD 4° branches were precisely colocalized with SAX-7 stripes (30 out of 30 animals examined), suggesting that the SAX-7 stripes might instruct the pattern of the PVD 4° branches (Fig. 1A–D).

Two sets of evidences support this model. First, the SAX-7 stripes were clearly visible in L3 animals during development. However, at the same stage, the PVD 4° branches were not yet developed, indicating that the SAX-7 stripes were present before the outgrowth of the PVD

4° branches (Fig. 1F–I). Second, the 4° branches nearly completely failed to form in the *sax-7*(*nj48*) mutants, consistent with the notion that SAX-7 was necessary for the 4° branches (Fig. 1J and K). Since the 3° dendrite growth was also severely compromised in the *sax-7* mutants, it is difficult to conclude that the SAX-7 pattern in the muscle area instructs the 4° branch pattern based on this allele.

We took the following steps to further prove that the SAX-7 pattern in the muscle region is necessary and sufficient to guide 4° branch development. First, we looked for a genetic manipulation that rescued the SAX-7 expression in the location of the 3° dendrites but not at the 4° dendrites. To do this, we expressed SAX-7 in the PLM and ALM neurons in *sax-7* null mutants. The neurites of PLM and ALM were localized at the sublateral nerve cord coinciding with the 3° dendrites. With this transgene, the SAX-7 expression was achieved along the 3° dendrite but completely absent in the 4° dendrite region. Indeed, we found that this transgene could robustly rescue the 3° dendrite phenotype but no 4° dendrite formed. We also noticed that the growth of PVD dendrite in this background stringently followed the trajectory of PLM and ALM (Fig. S1). This data argues that the SAX-7 expression in the muscle region is required for 4° dendrite even when the 3° dendrites are intact.

Second, we sought to generate an artificial pattern of SAX-7 in the muscle area to test if it could direct the pattern of the 4° branches. To achieve this, we co-expressed SAX-7 and MNR-1 in the D type neurons (DD and VD) and the PLM/ALM neurons in *sax-7; mnr-1* double mutants. The D type neurons have dorsoventrally oriented commissures that traverse the muscle area. We found that this combination of transgenes caused the PVD dendrite to grow both 3° and 4°-like dendrite. Again, the 4°-like dendrite stringently followed the commissures. This gain-of-function experiment argues that an ectopic pattern of SAX-7 in the muscle area leads to a predictable pattern of the PVD 4° branches (Fig. S1, Dong et al., 2013). Together, these data strongly support the idea that SAX-7 stripes provide the instructive cues for the outgrowth or stabilization of the PVD 4° branches, similar to its function in guiding the growth of 3° branches.

The SAX-7 stripes outnumbered the PVD 4° branches, creating two populations of SAX-7 stripes, the dendrite associated stripes and the “free” ones. Moreover, the intensity of the dendrite associated SAX-7 stripes were consistently stronger than the free stripes, raising the possibility that only the stronger SAX-7 stripes had the ability to attract dendrites (Fig. 1B–D). To test if there were fundamental differences between the two types of SAX-7 stripes in guiding PVD dendrites, we examined a mutant *wy50001* with five PVDs on each side of the worm instead of one on each side in wild type animals (Fig. S2A and B). This mutant was isolated in a forward genetic screen and mapped to the transcription factor LIN-22 (see material and method). In the wild type animals, around 40% of the SAX-7 stripes were associated with the PVD dendrites. In *lin-22*(*wy50001*) mutants, significantly more 4° branches formed most likely due to the additional PVD neurons, which occupied more than 80% of the SAX-7 stripes (Fig. S2C–F). This result suggests that most (if not all) of the SAX-7 stripes are competent to guide PVD dendrites. Interestingly, the “stronger” SAX-7 stripes were also associated with the PVD dendrites in this mutant background, raising the possibility that association with the dendrites increased the SAX-7 intensity.

To definitely test this hypothesis, we examined the SAX-7 stripes in the *dma-1* mutant that completely lacked the 4° branches. Indeed, in *dma-1* animals, the intensity of the SAX-7 stripes became more uniformly (Fig. S1). Since DMA-1 is the neuronal receptor for SAX-7 in PVD (Dong et al., 2013; Liu and Shen, 2012), it is plausible that DMA-1 can recruit SAX-7 and form “strong” stripes. Together, these data are consistent with the model that the pre-patterned SAX-7 stripes in the hypodermis guide the branching and growth of the PVD 4° branches.

unc-52 mutants show reduced, disorganized 4° branches and abnormal SAX-7 stripes

To further understand how SAX-7 is localized to these stripes and how the 4° branches form, we performed a RNAi and candidate mutants screen for mutants with altered PVD morphology. We found that perturbation of the basement membrane protein UNC-52/Perlecan disrupted PVD 4° branches specifically without affecting the PVD axon or the 1°, 2° and 3° branches (Fig. 2A–E). In *unc-52*(*e1421*) mutant, the number of PVD 4° branches was greatly reduced, with ~80% menorahs containing less than three 4° branches (Fig. 2E). Whereas in wild type animals only ~30% menorahs contained less than three 4° branches (Fig. 2E). In *unc-52*(*e1421*) mutant, the remaining 4° branches also exhibited abnormal turning or branching, resulting in the “L” or “T”-shaped branches instead of the “I” shape in the wild type animals (Fig. 2A–C). More than 40% of the 2° branches contained “L” or “T”-shaped in *unc-52*(*e1421*) mutants, compared to ~2% in wild type animals (Fig. 2D). Another *unc-52* allele, *e998* showed a similar phenotype as *e1421* (Fig. S3). *unc-52* possesses a number of isoforms created by alternative splicing (Rogalski et al., 2001). A third *unc-52* allele *gk3*, specificially lacking the long isoform of UNC-52, did not show any visible PVD branching phenoptye (Fig. S3), indicating the medium and/or short isoforms of UNC-52 were sufficient to support PVD branching. Consistent with these results, feeding RNAi of *unc-52* also produced similar PVD 4° branches phenotype as *unc-52* alleles (data not shown), indicating that loss of UNC-52 causes reduced and misguided 4° branches.

Next, we asked if the SAX-7 stripes are also dependent on UNC-52. In both *unc-52*(*e1421*) and *unc-52*(*e998*) mutants, the regular SAX-7::YFP stripes pattern were largely absent. Sparse dim YFP stripes remained in the muscle but became curved and lacked obvious patterns (Fig. 2G, and Fig. S3). Remarkably, the disorganized SAX-7 lines were still associated with the abnormal PVD 4° branches (Fig. 2H, and Fig. S3), strongly suggesting that the dendrites followed the SAX-7 pattern even in the *unc-52* mutants. Transgenic animals expressing a *unc-52* genomic DNA fragment fully rescued both the SAX-7 localization phenotype as well as the PVD dendrite phenotypes in *unc-52*(*e1421*) mutants (Fig. 2D–E and I–K). Together, these data strongly suggest that UNC-52 is required for the regular SAX-7 stripes which then guides the PVD 4° branches.

Pre-patterned UNC-52 orients SAX-7 subcellular localization

UNC-52 is a heperan sulfate proteoglycan synthesized by the hypodermis and muscle and deposited at the basement membrane (Mullen et al., 1999; Rogalski et al., 1993; Spike et al., 2002). Located between the muscle and hypodermis, UNC-52 covers the entire muscle quadrant but is concentrated at muscle-muscle cell boundaries and at the dense body (DB) and M-line of sarcomeres in the muscle cells, forming puntate rows (DB’s) and and narrow

stripes (M-line's) (Francis and Waterston, 1991). UNC-52 anchors the DB and M-lines at the muscle plasma membrane through integrin complexes (Mullen et al., 1999; Rogalski et al., 1993). To understand the relationship between UNC-52 and SAX-7, we performed double staining experiments using the MH3 antibody (against UNC-52) and a GFP antibody (SAX-7::YFP). Despite the similar regularly spaced stripe-like localization pattern of both molecules, we found that the SAX-7 (green) signal and UNC-52 (red) signal rarely overlapped with each other (Fig. 3A–C). Instead, the SAX-7 stripes were intercalated between the longitudinally aligned UNC-52 puncta, as shown in the line profiles of different fluorescence channels (Fig. 3A–C, and G). Consistent with this result, the PVD 4° branches also lied between the UNC-52 stained lines as shown by PVD::GFP and staining with another UNC-52 specific antibody (GM1) (Fig. 3D–F, and H). To ask if SAX-7 is required for the UNC-52 pattern, we examined the UNC-52 staining in *sax-7*(*nj48*) mutant with the GM1 antibody and found that the UNC-52 pattern was indistinguishable from that of the wild type (Fig. S4). Together, these results indicate that the sarcomere structure patterns an adhesion molecule SAX-7 in the hypodermis through the extracellular UNC-52/Perlecan, which in turn instructs the growth and branching of sensory dendrite terminals.

At the basement membane, UNC-52 is linked to the dense body and M-line of the sarcomeres through an integrin complex at the muscle plasma membrane (Rogalski et al., 1993). This integrin complex contains the the PAT-2/PAT-3 integrins (Gettner et al., 1995), along with several other proteins, including the kindlin homolog, UNC-112 (Rogalski et al., 2000). We next asked whether the integrin complex is required for the SAX-7 pattern and PVD dendrite formation. Postembryonic feeding RNAi of either *pat-2* (60% penetrance) or *unc-112* (100% penetrance) showed reduced and abnormally shaped 4° dendrite phenotypes that were reminiscent of the *unc-52* mutants (Fig. 4A–C, and J). While the SAX-7 stripes were still present, the stripe pattern was abnormal with frequent curved lines, which tightly correlated with the misguided PVD branches (Fig. 4D–I). These results suggest that the dense body and M-line components in the muscle also influence the patterning of SAX-7 stripes and PVD 4° branches possibly through anchoring UNC-52. The SAX-7 localization phenotype was less pronouced in the *pat-2* and *unc-112* RNAi animals compared with the *unc-52* mutants, possibly due to the variable effectiveness of RNAi in knocking down the endogenous genes.

The SAX-7 subcellular localization pattern requires its intracellular domain

Since SAX-7 functions in the hypodermal cell to guide the PVD dendrites through direct interactions with neuronal receptor DMA-1 (Dong et al., 2013), the next question is how UNC-52 patterns the subcellular organization of SAX-7 in the hypodermal cells. First, we used a structure-function approach to understand which domains of SAX-7 are required for its localization and function. A truncated construct, SAX-7(ΔExtra)::YFP, lacking all four Ig domains and five FnIII domains of the extracellular domain of SAX-7 could still localize as stripes but failed to rescue *sax-7* mutant phenotype (Fig. 5A–D and data not shown). Therefore, the extracellular domain was essential for guiding PVD dendrites, and the cytoplasmic domain of SAX-7 might be sufficient to localize it to the hypodermal stripes. Consistently, a truncated SAX-7 construct lacking the entire cytosolic domain, SAX-7(ΔCyto)::YFP failed to form stripes and was instead diffusely localized on the plasma

membrane (Fig. 5E–H). Together, these data strongly suggest that the cytoplasmic domain of SAX-7 localizes the protein to the stripes in the hypodermal cells.

Since the fluorescence intensity of SAX-7::GFP at the sublateral line was much higher than at the stripes underneath the muscles (Fig. 1C), we tested if the "affinity" of sublateral lines for SAX-7 might be higher compared to that of the 4° stripes. Transgene animals in which P*dpy-7*::SAX-7::YFP was injected at a low concentration (0.1ng/μL) partially rescued the PVD 3° branch phenotype of the *sax-7*(*nj48*) mutants but not the 4° branches (Fig. 5I–L). This transgene showed faint SAX-7::YFP at sublateral lines but not the stripes in the 4° branch region. This result implies that low amount of SAX-7 preferentially localized to the sublateral line rather than to the 4° branch locations.

Hypodermal fibrous organelle (FO) orients SAX-7 subcellular localization

Signaling from body wall muscle is known to directly organize the hemi-desmosomes in the hypodermal cells, which are called fibrous organelle (FO) complexes in *C. elegans* (Hresko et al., 1999). FOs and hemidesmosomes are conserved attachment complexes that connect the epithelial cell cytoplasm to the extracellular matrix using intermediate filaments. These adhesion complexes are thought to provide tissue integrity and resistance to mechanical forces (Zhang and Labouesse, 2010). Because the FOs are known to form regular stripe pattern, we examined the relationship between the FOs and the patterns of UNC-52 and SAX-7 stripes. Using a MUA-6::mCherry marker, which is the intermediate filaments component of FOs, we found that both MUA-6::mCherry and SAX-7::GFP showed strikingly similar stripe patterns in the same part of the hypodermis underneath the muscles. Remarkably, the MUA-6 stripes precisely interdigitated with the SAX-7 stripes (Fig. 6A–C). Hence, the FOs and SAX-7 occupied alternating subcellular domains on the hypodermal cells and were mutually exclusive of each other. As PVD 4° branch always followed SAX-7 stripes, we also examined the relationship between the MUA-6 stripes and the PVD 4° branches. Not surprisingly, all 4° branches localized between the MUA-6 stripes (Fig. 7A–C), consistent with the interdigitating localization between MUA-6 and SAX-7.

The precise complementary localization patterns of SAX-7 and MUA-6 prompted us to test if there is any causal relationship between the FO components and the SAX-7 stripes. First, we examined the SAX-7 and MUA-6 localization during development. In newly hatched worms, the MUA-6 stripes were readily detectable while the SAX-7 stripes were not formed, suggesting that FOs might pattern the SAX-7 stripes (Fig. 6D–F). Second, In *mua-6(rh85)* mutant the regular SAX-7 stripes disappeared and the PVD 4° branches were largely absent (Fig. 6G–I), indicating that the intact FO structure might be required to form the SAX-7 stripes, which then instructed the pattern of PVD branches. Because the SAX-7 stripes were adjacent to but did not overlap with the MUA-6 stripes, we next asked if MUA-6 intermediate filament excludes SAX-7. Overexpression of MUA-6::mCherry led to partial disappearance of the SAX-7 stripes and much reduced PVD 4° branches (Fig. 6J–L, and Fig. S5). In cases where the overexpression was not uniform within a single animal, locations with high level of MUA-6::mCherry strongly correlated with lack of SAX-7 stripes (arrow in Fig. 6J–L), while the SAX-7 stripes were still present at neighboring areas

with low MUA-6::mCherry (arrowhead in Fig. 6J–L). These findings suggest that the existing MUA-6 stripes in the hypodermal cells pattern the SAX-7 by locally excluding it.

To further test this hypothesis, we examined the localization of MUA-6 and PVD dendrites in *unc-52* mutants. Since UNC-52 is important to anchor the hemidesmosomes and PVD 4° branches exhibit specific defects in *unc-52* mutant, we asked if the MUA-6 stripe pattern is affected in the *unc-52* mutants. In the partial loss-of-function *unc-52* alleles, we found that all the mutants exhibited disorganized MUA-6 stripes with broken circumferential stripes and irregularly shaped holes and gaps. Strikingly, most of the abnormally shaped PVD dendrites (about 80% in 15 observed animals) precisely coincided with the gaps in the MUA-6 staining (Fig. 7D–F). Furthermore, most of the abnormally shaped SAX-7 stripes also localized to the MUA-6 holes and gaps (Fig. 7G–I). Together, these data support the model that the extracellular matrix protein UNC-52 forms regular stripes following the muscle sarcomeres and is essential for the formation of regular hemi-desmosome structures on the hypodermal cells, which in turn patterns the SAX-7 stripes by locally excluding the SAX-7 localization. Subsequently, the SAX-7 utilizes its ectodomain to instruct the growth of the PVD 4° branches by interacting with DMA-1 and MNR-1.

Discussion

Our results provided a concrete model for the development of the PVD dendrites. While the 3° branches are instructed by the sublateral stripes of SAX-7, the 4° branches were precisely guided by circumferential stripes of SAX-7 on the hypodermal membrane underneath the muscle cells. The precise co-localization between the SAX-7 stripes and the PVD 4° branches and the complete lack of 4° branches in the *sax-7*, *mnr-1* or *dma-1* mutants demonstrate that the pre-patterned SAX-7 stripes instructed the development of PVD dendrites. Consistent with our previous findings, the SAX-7 signal is detected by the PVD receptor DMA-1. This recognition also requires co-ligand MNR-1 on the hypodermal cells. Since DMA-1 is specifically expressed in the PVD neurons, but not in many other neurons that extend neurites along the hypodermal cells, only PVD develops exuberant branches.

Here, we provided a satisfying explanation to how the SAX-7 stripes are localized to specific parts of the hypodermal cells with a distinct pattern. Our genetic analysis demonstrates that UNC-52/Perlecan is important for patterning the SAX-7 stripes and the PVD dendrite. In *unc-52* mutants, both the SAX-7 stripes and the PVD 4° branches were disorganized. Interestingly, the disorganized PVD 4° branches still followed the disrupted SAX-7 stripes, strongly suggesting that SAX-7 patterns dictate the PVD dendrite morphology. UNC-52 is only detected in the basement membrane associated with muscle cells and it is concentrated beneath the muscle dense bodies (DB) and M-lines under body wall muscles (Francis and Waterston, 1991; Mullen et al., 1999; Rogalski et al., 1993). This explains why the PVD 4° branches only develop underneath the muscle cells but not at more medial locations.

UNC-52 plays essential functions to link the sarcomere structure in the muscle to specific subcellular hemi-desmosomes in the hypodermal cells. At the muscle plasma membrane, UNC-52 binds to the dense bodies and M lines through integrin complexes. At the

hypodermal cell membrane, UNC-52 is important for patterning LET-805 and hemi-desmosome, fibrous organelles (FOs) (Cox and Hardin, 2004; Francis and Waterston, 1991). Our genetic epistasis analyses demonstrated a developmental hierarchy. UNC-52 is essential for the subcellular localization of the hemi-desmosome, including the intermediate filament MUA-6. MUA-6 in turn patterns SAX-7, likely through the interaction with the cytosolic domain of SAX-7. SAX-7 uses its extracellular domain, together with MNR-1 to attract PVD dendrite growth and stabilization by binding to DMA-1. This model highlights the importance of cell-cell interactions in the morphogenesis of neurons. In *Drosophila* class IV dendritic arborization (da) neurons integrin-laminin interaction attaches dendrites to the ECM (Han et al., 2012; Kim et al., 2012). Disruption of such interactions causes the dendrite to be embedded in the epidermis. In another related study, Yasunaga et al., showed that the degradation of basement membrane components by Mmp2 is required to reshape dendrite during development of *Drosophila* (Yasunaga et al., 2010). Similarly, HSPGs in zebrafish play important roles in guiding the peripheral axons to innervate the skin (Wang et al., 2012), suggestive of an evolutionarily conserved mechanism of peripheral neurite patterning by ECM molecules.

PVD is postulated to function as a proprioceptor, sensing and controlling body posture, based on the abnormal posture caused by ablating PVD (Albeg et al., 2011). Our hypothesis not only demonstrates the mechanism of PVD 4° dendrites development through muscle derived cues, but also illustrates the close association between the sarcomere and the PVD dendrites. In addition, it is worth noting that the hemi-desmosome like fibrous organelle is thought to act as tendon like structures that transmit tension of muscle contraction to cuticle. Thus, this developmental program utilizes the UNC-52/Perlecan and SAX-7 to bundle the tension transmitting cell junctions with a proprioceptive sensory dendrite.

The best-understood mammalian proprioceptive receptor is the muscle spindle. Similar to the hypodermal-muscle-dendrite complex in PVD, the muscle spindle contains the sheath cells, specialized muscle fibers and nerve terminals. The sensory nerve terminals wrap around the muscle cells several rounds with evenly spaced turns. Remarkably, in both worms and mammals, the sensory nerves are oriented perpendicular to longitudinal axis of the sarcomeres, a configuration that might maximize the stretching effects from the muscle onto the nerve (Cheret et al., 2013). Future studies are needed to test if the cellular and molecular interactions that we described here play a similar role in patterning the muscle spindles.

Experimental Procedures

C. elegans Strains, Genetics and RNAi

C. elegans strains were cultured at 20°C on NGM (Nematode Growth Medium) plates seeded with the *Escherichia coli* OP50 using standard methods(Brenner, 1974). All the mutants and transgene strains were genetically modified from the wild type strain N2. *wy50001* was isolated from a forward genetic screen for PVD dendrite morphology defect. Genetic mapping and sequence showed that *wy50001* is a nonsense mutation of W62 in the *lin-22* gene. *mua-6* (*rh85*) is partial lethal and the survival worms are very sick. Strains used were listed in Table S1. Standard feeding RNAi was used to knock down genes using the

RNAi feeding library (Fraser et al., 2000). Synchronized L1 worms were transferred to RNAi feeding plates (*unc-112*, *pat-2*), and young adults were observed 3 days later. The penetrance is the percentage of animals showing PVD dendrite defects in total animals observed.

Molecular Biology and Transgenes

PCR and molecular cloning techniques were used to generate fluorescence reporters. The PCR products were amplified with Phusion DNA polymerase (New England Biolabs) or TransStart® FastPfu DNA Polymerase (Transgen Biotech). The plasmids were constructed using the Clontech In-Fusion® PCR Cloning System and verified by sequencing. The plasmid constructs are listed in Table S2. Transgenic worms were constructed through germ-line transformation using microinjection technique. The DNA plasmids and PCR products were injected at 5–50 ng/μl into N2 hermaphrodites with a fluorescent selection marker (such as P*odr-1*::GFP). At least two independent lines were isolated and analyzed for the data.

Quantitation and Statistics

The data were expressed, unless otherwise mentioned, as the mean ± SEM. The statistic tests were either two-tailed Student's t-test or one-way ANOVA (The Analysis Of Variance). The p values are indicated by asterisks in the figures legends with the following notations: * $p \leq 0.05$; ** $p \leq 0.01$; *** $p \leq 0.001$.

Fluorescent Imaging

Young adult animals were anesthetized by 1mg/ml levamisole in M9 buffer, and then mounted on 3% (wt/vol) agar pads. Images of fluorescent proteins were captured in live animals using a 40x objective on an AxioImager M2 microscope (Carl Zeiss). The spinning disk confocal imaging system includes an Axio Observer Z1 microscope (Carl Zeiss MicroImaging) equipped with a 40× and a 100 ×, objective, an EM CCD camera (Andor), and the 488-, and 568-nm lines of a Sapphire CW CDRH USB Laser System attached to a spinning disk confocal scan head (Yokogawa CSU-X1 Spinning Disk Unit). The confocal images were taken with Micro-Manager (www.micro-manager.org) software. ImageJ (http://rsbweb.nih.gov/ij/) software was used to process the images.

Antibody staining

Antibody staining was performed with whole-mount worms using standard protocol (Qin et al., 2014; Zhou et al., 2008). For the SAX-7 antibody, the "Freeze-cracking" method was used to increase tissue accessibility, and the worms were fixed by methanol/acetone (Duerr, 2006). For immunofluorescence detection of endogenous UNC-52 and SAX-7::YFP, worms were incubated with anti-UNC-52(MH3 or GM1) and anti-GFP antibody simultaneously. The UNC-52-specific antibody GM1 was kindly provided by Dr. Moerman, and the UNC-52-specific antibody MH3 was from DSHB, Rabbit polyclonal 6991 antibody against the SAX-7 cytoplasmic tail was kindly provided by Dr. Lihsia Chen at University of Minnesota. Rabbit polyclonal antibody against GFP (genscript) was used to detect the

P*dpy-7*::SAX-7::YFP. Antibodies against UNC-52 or GFP were used at 1:200 dilution. Antibody against SAX-7 was used at 1:300 dilution.

Supplementary Material

Refer to Web version on PubMed Central for supplementary material.

Acknowledgements

We are grateful to the *Caenorhabditis* Genetics Center and Dr. G.S. Ou for strains and Dr. M. Ding for technical help of antibody staining, Dr. L.S. Chen for SAX-7 antibody. This work was supported by the National Basic Research Program of China (2013CB910103), the Howard Hughes Medical Institute and NINDS (1R01NS082208) to K. Shen, and a grant from the NSFC (31201048, 31428009) to X.M. Wang and K. Shen, and the CAS/SAFEA International Partnership Program for Creative Research Teams to K. Shen. Work in the laboratory of DGM was supported by the Canadian Institute for Health Research. DGM is a Fellow of the Canadian Institute for Advanced Research.

References

Brenner S. The genetics of Caenorhabditis elegans. Genetics. 1974; 77(1):71–94. [PubMed: 4366476]

Fraser AG, Kamath RS, Zipperlen P, Martinez-Campos M, Sohrmann M, Ahringer J. Functional genomic analysis of C. elegans chromosome I by systematic RNA interference. Nature. 2000; 408(6810):325–330. [PubMed: 11099033]

Albeg A, Smith CJ, Chatzigeorgiou M, Feitelson DG, Hall DH, Schafer WR, Miller DM 3rd, Treinin M. C. elegans multi-dendritic sensory neurons: morphology and function. Molecular and cellular neurosciences. 2011; 46:308–317. [PubMed: 20971193]

Arikkath J. Molecular mechanisms of dendrite morphogenesis. Frontiers in cellular neuroscience. 2012; 6:61. [PubMed: 23293584]

Bewick GS, Banks RW. Mechanotransduction in the muscle spindle. Pflugers Archiv : European journal of physiology. 2014

Brenner S. The genetics of Caenorhabditis elegans. Genetics. 1974; 77:71–94. [PubMed: 4366476]

Chatzigeorgiou M, Yoo S, Watson JD, Lee WH, Spencer WC, Kindt KS, Hwang SW, Miller DM 3rd, Treinin M, Driscoll M, Schafer WR. Specific roles for DEG/ENaC and TRP channels in touch and thermosensation in C. elegans nociceptors. Nature neuroscience. 2010; 13:861–868. [PubMed: 20512132]

Cheret C, Willem M, Fricker FR, Wende H, Wulf-Goldenberg A, Tahirovic S, Nave KA, Saftig P, Haass C, Garratt AN, Bennett DL, Birchmeier C. Bace1 and Neuregulin-1 cooperate to control formation and maintenance of muscle spindles. The EMBO journal. 2013; 32:2015–2028. [PubMed: 23792428]

Corty MM, Matthews BJ, Grueber WB. Molecules and mechanisms of dendrite development in Drosophila. Development. 2009; 136:1049–1061. [PubMed: 19270170]

Cox EA, Hardin J. Sticky worms: adhesion complexes in C. elegans. Journal of cell science. 2004; 117:1885–1897. [PubMed: 15090594]

Dong X, Liu OW, Howell AS, Shen K. An extracellular adhesion molecule complex patterns dendritic branching and morphogenesis. Cell. 2013; 155:296–307. [PubMed: 24120131]

Duerr JS. Immunohistochemistry. WormBook : the online review of C. elegans biology. 2006:1–61. [PubMed: 18050446]

Francis R, Waterston RH. Muscle cell attachment in Caenorhabditis elegans. The Journal of cell biology. 1991; 114:465–479. [PubMed: 1860880]

Fraser AG, Kamath RS, Zipperlen P, Martinez-Campos M, Sohrmann M, Ahringer J. Functional genomic analysis of C. elegans chromosome I by systematic RNA interference. Nature. 2000; 408:325–330. [PubMed: 11099033]

Gettner SN, Kenyon C, Reichardt LF. Characterization of beta pat-3 heterodimers, a family of essential integrin receptors in C. elegans. The Journal of cell biology. 1995; 129:1127–1141. [PubMed: 7744961]

Han C, Wang D, Soba P, Zhu S, Lin X, Jan LY, Jan YN. Integrins regulate repulsion-mediated dendritic patterning of drosophila sensory neurons by restricting dendrites in a 2D space. Neuron. 2012; 73:64–78. [PubMed: 22243747]

Hresko MC, Schriefer LA, Shrimankar P, Waterston RH. Myotactin, a novel hypodermal protein involved in muscle-cell adhesion in Caenorhabditis elegans. The Journal of cell biology. 1999; 146:659–672. [PubMed: 10444073]

Ikeda R, Cha M, Ling J, Jia Z, Coyle D, Gu JG. Merkel cells transduce and encode tactile stimuli to drive Abeta-afferent impulses. Cell. 2014; 157:664–675. [PubMed: 24746027]

Jan YN, Jan LY. Branching out: mechanisms of dendritic arborization. Nature reviews. Neuroscience. 2010; 11:316–328. [PubMed: 20404840]

Kim ME, Shrestha BR, Blazeski R, Mason CA, Grueber WB. Integrins establish dendrite-substrate relationships that promote dendritic self-avoidance and patterning in drosophila sensory neurons. Neuron. 2012; 73:79–91. [PubMed: 22243748]

Liu OW, Shen K. The transmembrane LRR protein DMA-1 promotes dendrite branching and growth in C. elegans. Nature neuroscience. 2012; 15:57–63. [PubMed: 22138642]

Mullen GP, Rogalski TM, Bush JA, Gorji PR, Moerman DG. Complex patterns of alternative splicing mediate the spatial and temporal distribution of perlecan/UNC-52 in Caenorhabditis elegans. Molecular biology of the cell. 1999; 10:3205–3221. [PubMed: 10512861]

Oren-Suissa M, Hall DH, Treinin M, Shemer G, Podbilewicz B. The fusogen EFF-1 controls sculpting of mechanosensory dendrites. Science. 2010; 328:1285–1288. [PubMed: 20448153]

Qin J, Liang J, Ding M. Perlecan antagonizes collagen IV and ADAMTS9/GON-1 in restricting the growth of presynaptic boutons. The Journal of neuroscience : the official journal of the Society for Neuroscience. 2014; 34:10311–10324. [PubMed: 25080592]

Rogalski TM, Gilchrist EJ, Mullen GP, Moerman DG. Mutations in the unc-52 gene responsible for body wall muscle defects in adult Caenorhabditis elegans are located in alternatively spliced exons. Genetics. 1995; 139:159–169. [PubMed: 7535716]

Rogalski TM, Mullen GP, Bush JA, Gilchrist EJ, Moerman DG. UNC-52/perlecan isoform diversity and function in Caenorhabditis elegans. Biochemical Society transactions. 2001; 29:171–176. [PubMed: 11356148]

Rogalski TM, Mullen GP, Gilbert MM, Williams BD, Moerman DG. The UNC-112 gene in Caenorhabditis elegans encodes a novel component of cell-matrix adhesion structures required for integrin localization in the muscle cell membrane. The Journal of cell biology. 2000; 150:253–264. [PubMed: 10893272]

Rogalski TM, Williams BD, Mullen GP, Moerman DG. Products of the unc-52 gene in Caenorhabditis elegans are homologous to the core protein of the mammalian basement membrane heparan sulfate proteoglycan. Genes & development. 1993; 7:1471–1484. [PubMed: 8393416]

Salzberg Y, Diaz-Balzac CA, Ramirez-Suarez NJ, Attreed M, Tecle E, Desbois M, Kaprielian Z, Bulow HE. Skin-derived cues control arborization of sensory dendrites in Caenorhabditis elegans. Cell. 2013; 155:308–320. [PubMed: 24120132]

Smith CJ, O'Brien T, Chatzigeorgiou M, Spencer WC, Feingold-Link E, Husson SJ, Hori S, Mitani S, Gottschalk A, Schafer WR, Miller DM 3rd. Sensory neuron fates are distinguished by a transcriptional switch that regulates dendrite branch stabilization. Neuron. 2013; 79:266–280. [PubMed: 23889932]

Smith CJ, Watson JD, Spencer WC, O'Brien T, Cha B, Albeg A, Treinin M, Miller DM 3rd. Time-lapse imaging and cell-specific expression profiling reveal dynamic branching and molecular determinants of a multi-dendritic nociceptor in C. elegans. Developmental biology. 2010; 345:18–33. [PubMed: 20537990]

Spike CA, Davies AG, Shaw JE, Herman RK. MEC-8 regulates alternative splicing of unc-52 transcripts in C. elegans hypodermal cells. Development. 2002; 129:4999–5008. [PubMed: 12397108]

Wang F, Wolfson SN, Gharib A, Sagasti A. LAR receptor tyrosine phosphatases and HSPGs guide peripheral sensory axons to the skin. Current biology : CB. 2012; 22:373–382. [PubMed: 22326027]

Way JC, Chalfie M. The mec-3 gene of Caenorhabditis elegans requires its own product for maintained expression and is expressed in three neuronal cell types. Genes & development. 1989; 3:1823–1833. [PubMed: 2576011]

Woo SH, Ranade S, Weyer AD, Dubin AE, Baba Y, Qiu Z, Petrus M, Miyamoto T, Reddy K, Lumpkin EA, Stucky CL, Patapoutian A. Piezo2 is required for Merkel-cell mechanotransduction. Nature. 2014; 509:622–626. [PubMed: 24717433]

Yasunaga K, Kanamori T, Morikawa R, Suzuki E, Emoto K. Dendrite reshaping of adult Drosophila sensory neurons requires matrix metalloproteinase-mediated modification of the basement membranes. Developmental cell. 2010; 18:621–632. [PubMed: 20412776]

Zhang H, Labouesse M. The making of hemidesmosome structures in vivo. Developmental dynamics : an official publication of the American Association of Anatomists. 2010; 239:1465–1476. [PubMed: 20205195]

Zhou S, Opperman K, Wang XL, Chen LH. unc-44 Ankyrin and stn-2 gamma-Syntrophin Regulate sax-7 L1CAM Function in Maintaining Neuronal Positioning in Caenorhabditis elegans. Genetics. 2008; 180:1429–1443. [PubMed: 18791240]

Highlights

1. SAX-7/L1CAM in skin cells instructs branching of sensory dendrites.
2. SAX-7/L1CAM forms a regular striped pattern in skin cells.
3. The repeated sarcomeres pattern skin SAX-7 through ECM protein UNC-52/Perlecan.
4. Sarcomeres provide developmental cues for dendrite branching.

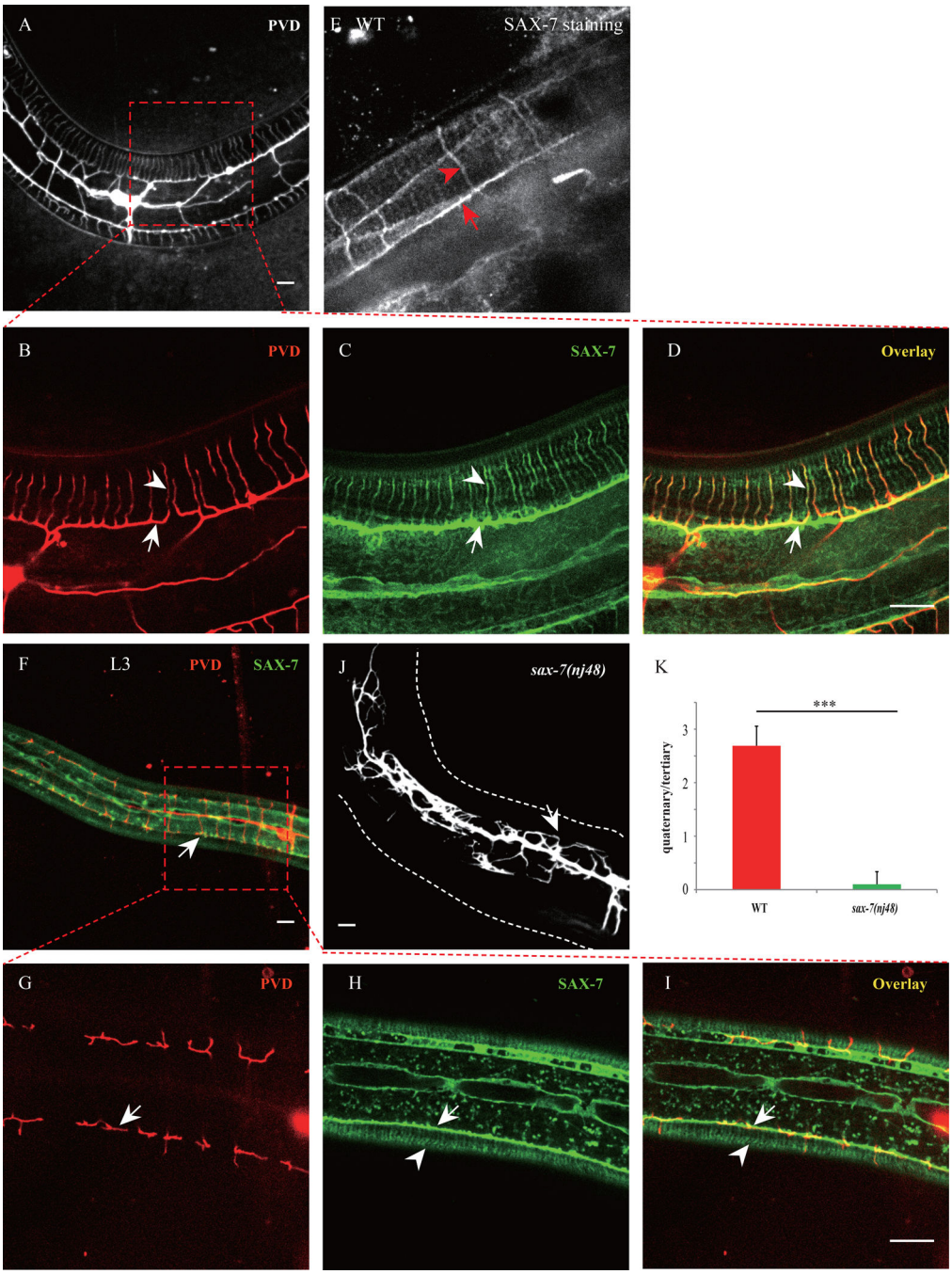

Fig. 1. Hypodermal SAX-7/L1CAM exhibits stripe-like patterns and co-localizes with the PVD 4° branches

A–D) Confocal images of a young adult animal expressing SAX-7::GFP under the control of the hypodermal cell promoter P*dpy-7*. PVD cells were labeled by mCherry. D) PVD quaternary branches (red) co-localized stringently with SAX-7 stripes (green). Arrows indicate the PVD tertiary branch and the SAX-7 sub-lateral stripe. Arrowheads mark one of the PVD 4° branches and the co-localized SAX-7 stripe. E). Wild type animal stained with SAX-7 antibody. Red arrow indicates the sublateral stripe and red arrowhead shows one

SAX-7 stripe around muscle quadrant. F–I) Confocal images of an L3 animal. Arrows indicate the positions of a PVD tertiary branch. Arrowheads mark the SAX-7 stripes underneath the muscles. Note that the SAX-7 stripes were present while the 4° branches were not yet developed at this stage. n=20. J) Confocal image of a *sax-7*(*nj48*) mutant expressing PVD::GFP. K) Quantification of PVD 4° branches phenotype of *sax-7*(*nj48*) mutant. Y-axis means the average ratio of 4° branches number / 3° branches number. Error bars, SEM. ***p < 0.001 by Student's t test. n=20. Scale bar is 10 μm.

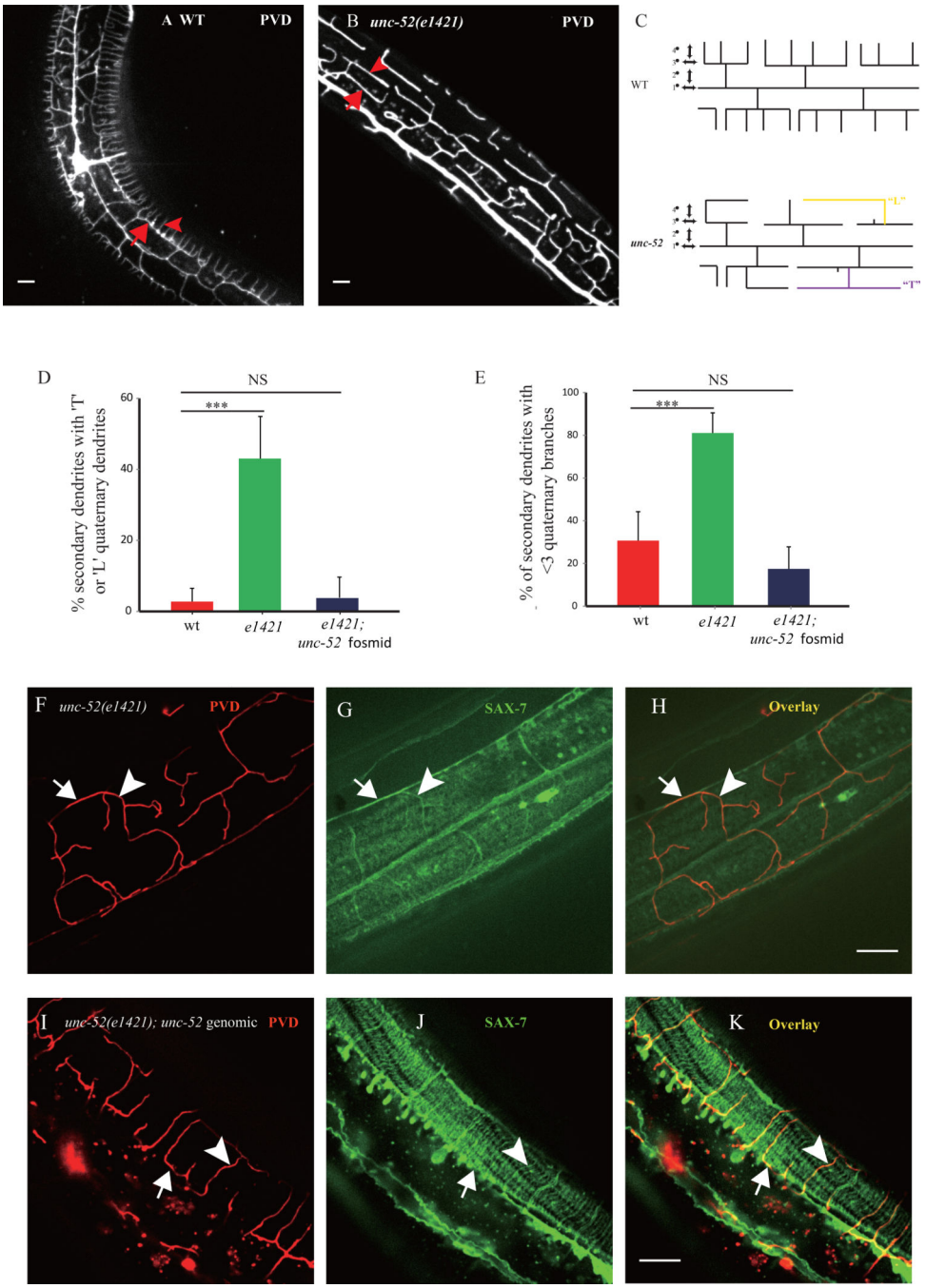

Fig. 2. *unc-52* mutant displays abnormal PVD 4° branches

A) Confocal image of wild type PVD morphology. Arrow indicates one 3° branch and the arrowhead shows one 4° branch. B) Confocal image of *unc-52*(*e1421*) mutant PVD morphology. Arrow indicates a 3° branch with fewer 4° branch, and the arrowhead shows a "T" shaped 4° branch. C) Schematic of wild type and *unc-52* mutant PVD neuron in the *C. elegans*. Note that WT PVD has straight 4° branches and that mutant PVD shows abnormal 4° branches that are labeled in yellow and purple. D) Quantification of the percentage of the 2° branches which contain "L" or "T" shaped 4° branches in *unc-52*(*e1421*) mutant and the

unc-52 genomic DNA rescued worms. E) Quantification of percentage of the 2° branches that contain less than three 4° branches in *unc-52*(*e1421*) mutant and the *unc-52* genomic DNA rescued worms. Error bars, SEM. ***p < 0.001 by ANOVA. NS: not significant. n>20 for each genotype. F–K) Confocal images of *unc-52*(*e1421*), and *unc-52*(*e1421*); *unc-52* genomic DNA rescued worms. In *unc-52*(*e1421*) mutants the disorganized SAX-7 stripes were always followed by the disorganized PVD 4° branches. Arrows indicate the PVD tertiary branch and the SAX-7 sub-lateral stripe. Arrowheads mark one of the PVD quaternary branch and the co-localized SAX-7 stripe.

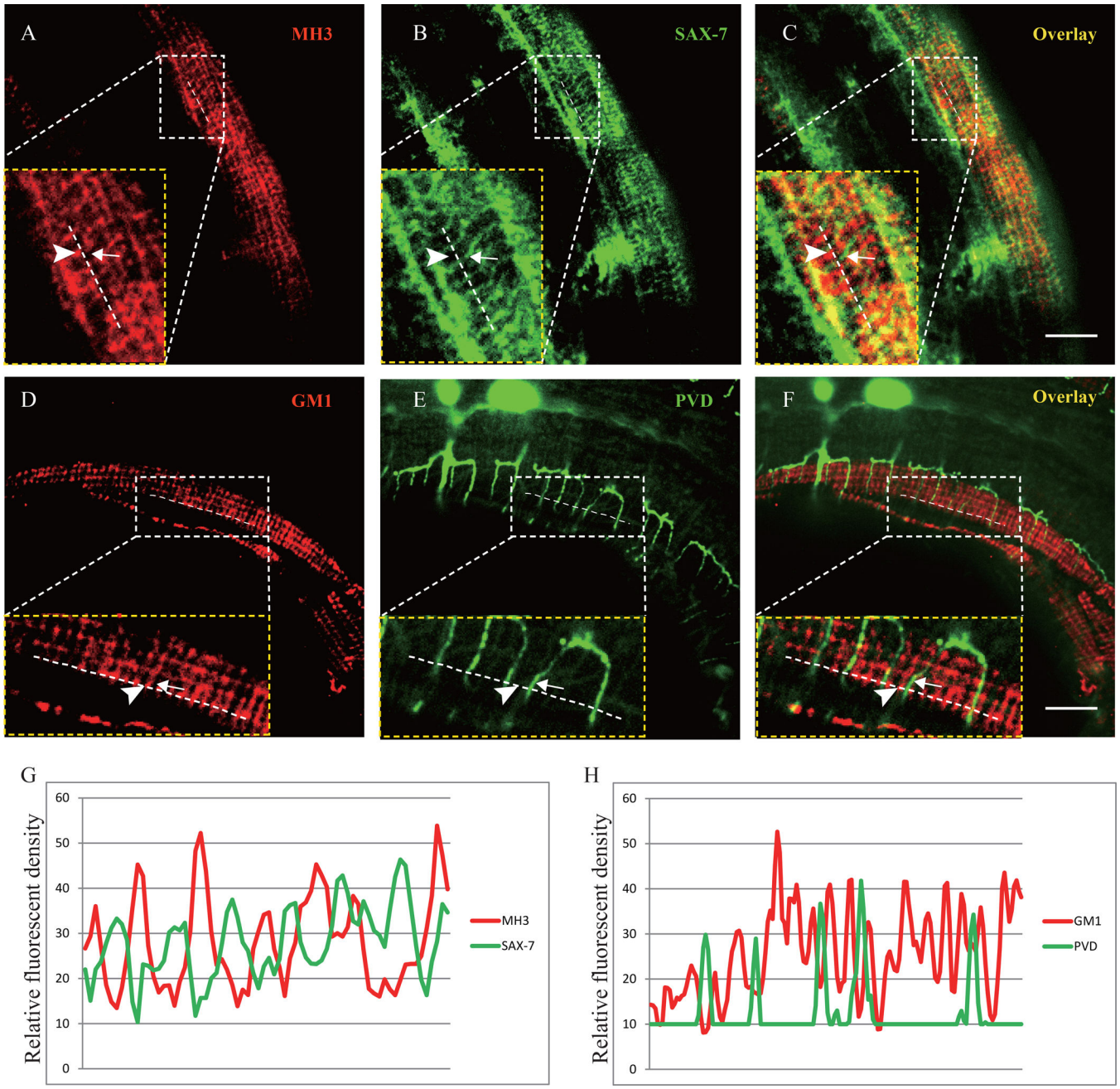

Fig. 3. UNC-52 and SAX-7 exhibit interdigitated localization pattern

A–C) Confocal images of SAX-7::GFP transgenic animal double stained with the MH3 (UNC-52) and GFP antibodies. The images of the inset are zooming in views of the region indicated by the box. Arrow points to the SAX-7 stripe and arrowhead marks the UNC-52 staining. D–F) Confocal images of a PVD::GFP animal strained with the GM1 (UNC-52) antibody. The images of the inset are zooming in views of the region indicated by the box. Arrows indicate the PVD 4° branch and arrowheads mark the UNC-52 staining. G) Line profiles of fluorescence intensity of UNC-52 and SAX-7. H) Line profiles of fluorescence intensity of UNC-52 and PVD::GFP. A clear staining region was chosen randomly to zoom

in and the schematic dotted line was drawn along the longitudinal UNC-52 puncta using ImageJ. The relative fluorescence intensity along the dotted lines in two channels (GFP and mCherry) was plotted to form the picture. Scale bar is 10 μm.

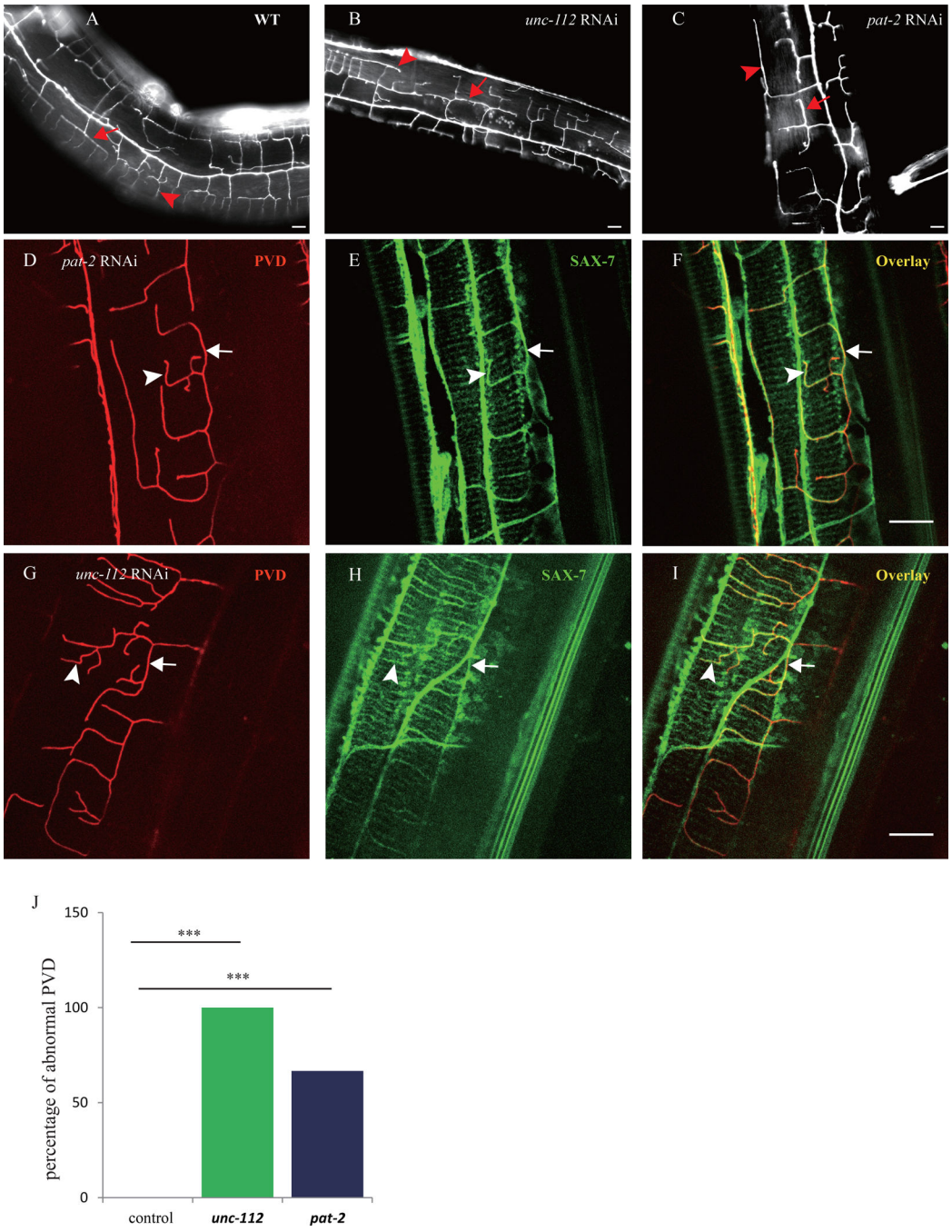

Fig. 4. Sarcomere components are important for the SAX-7 pattern and PVD branch morphology

A–C) Florescent images of PVD in young adult wild type and *unc-112* (RNAi), *pat-2* (RNAi) animals. D–I) Confocal images of PVD and P*dpy-7*::SAX-7::YFP of the *unc-112* (RNAi), *pat-2* (RNAi) animals. Arrows indicate the 3° branches and the SAX-7 lateral stripes. The arrowheads indicate the 4° branches and the co-localized SAX-7 stripes. J) Quantification of the RNAi penetrance. n>30 for each genotype. ***$p < 0.001$ by x^2 test. Scale bar is 10 μm.

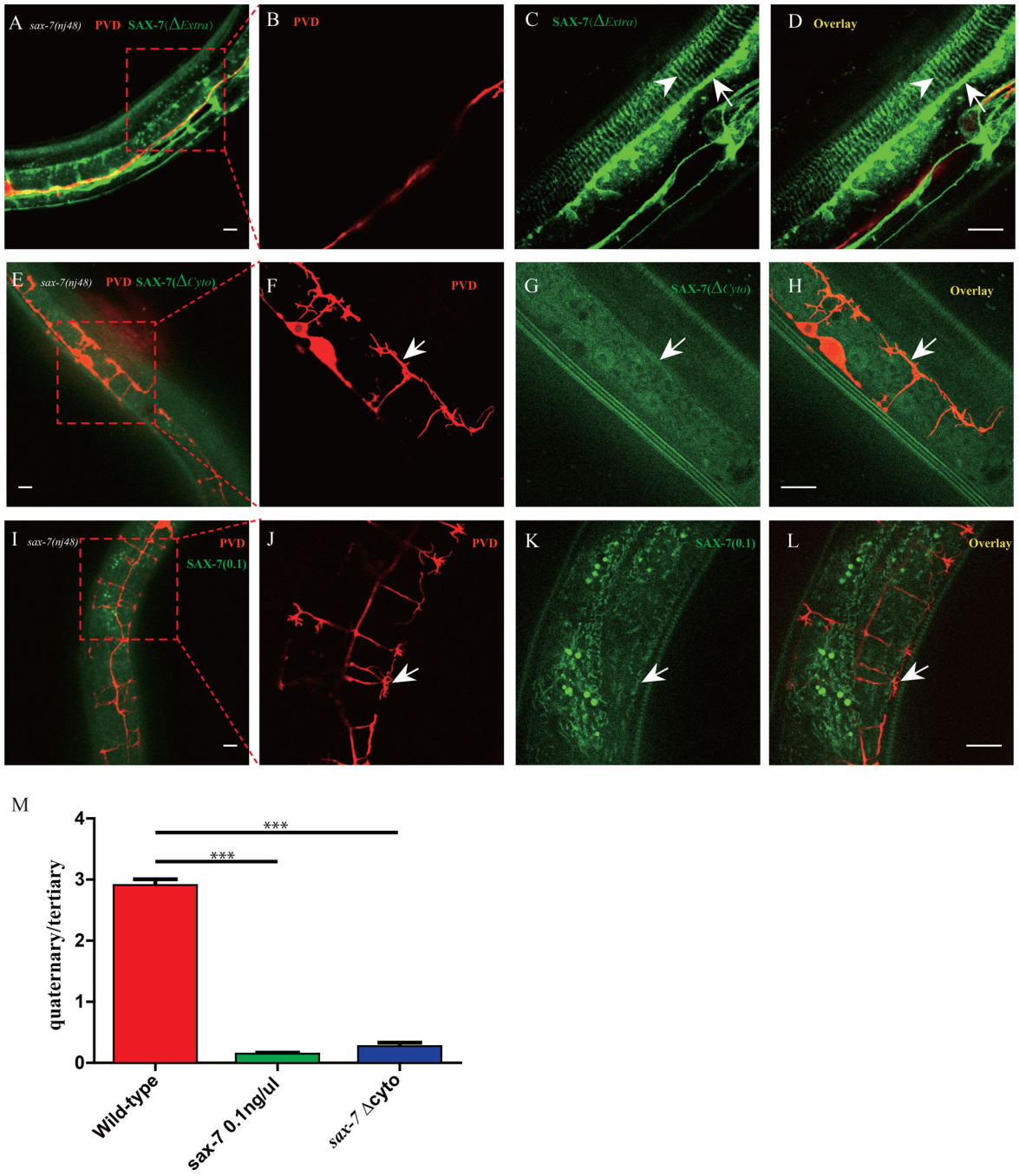

Fig. 5. Structure-function analysis of SAX-7

A–D) Confocal images of the P*dyp-7*::SAX-7(ΔExtra)::YFP transgene in *sax-7*(*nj48*) mutant. n>30. E–H) Confocal images of the P*dyp-7*::SAX-7(ΔCyto)::YFP transgene in *sax-7*(*nj48*) mutant. n>30. I–L) Confocal images of the P*dyp-7*::SAX-7::YFP(0.1ng/μl) transgene in *sax-7*(*nj48*) mutant. n>30. M) Quantification of rescue activity of SAX-7 truncation constructs in A) and I). Error bars, SEM. ***p < 0.001 by Student's t test, n>10 for each genotype. Scale bar is 10 μm.

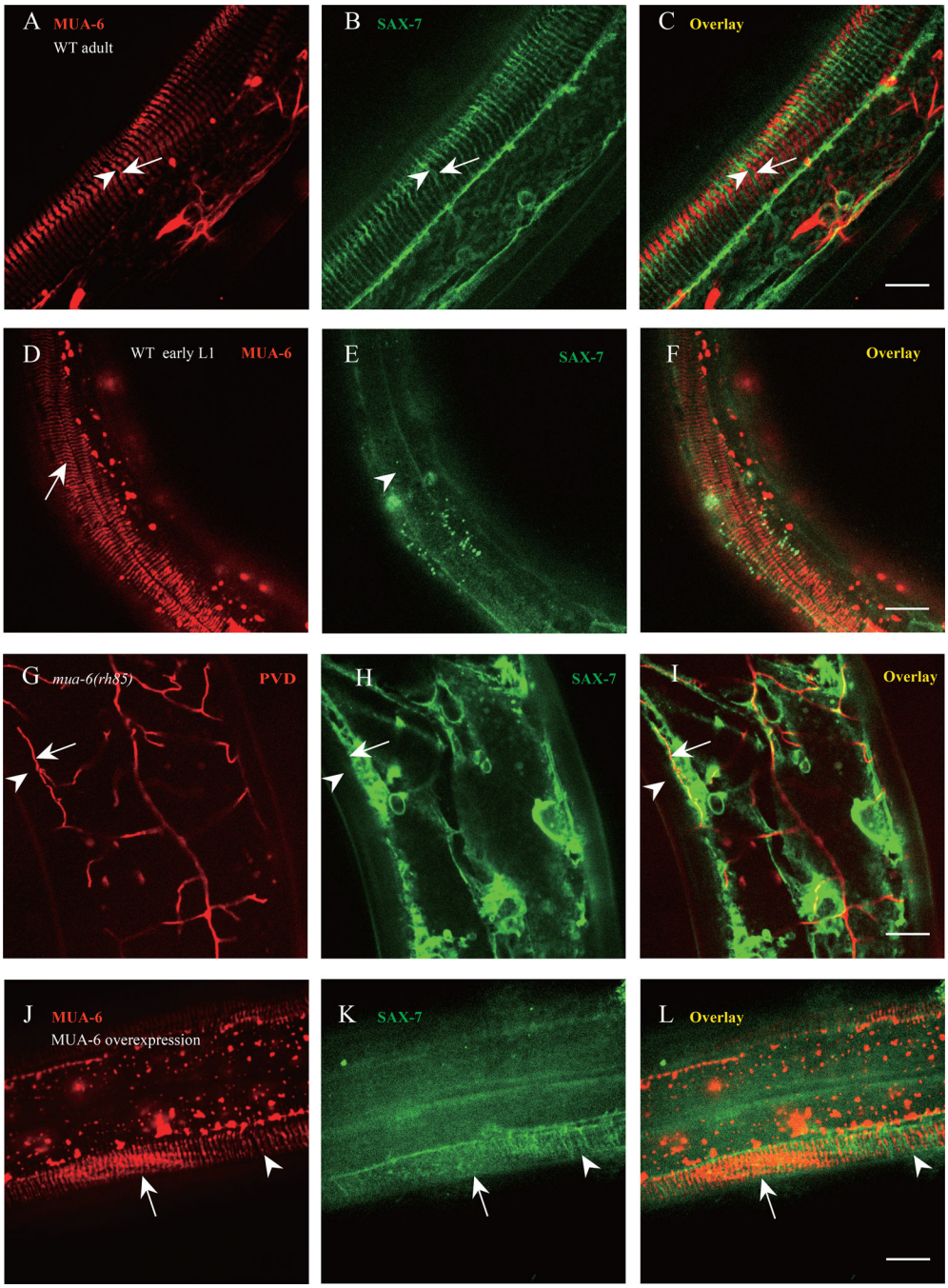

Fig. 6. Hypodermal FOs pattern SAX-7 stripes and then PVD 4° branches

A–C) Confocal images of the MUA-6::mCherry and SAX-7::GFP. Arrow indicates one FO stripe and arrowhead shows one SAX-7 stripe. n=30. D–F) Confocal images of the MUA-6::mCherry and SAX-7::GFP in a newly hatched L1 worm. Arrow indicates one FO stripe and arrowhead shows the region which SAX-7 stripe will form. n=20. G–I) Confocal images of the SAX-7::GFP and PVD::mCherry in *mua-6*(*rh58*) mutant. Arrows indicate PVD tertiary dendrite and arrowhead shows the region where SAX-7 stripe and PVD 4° branch should be. n=20. J–L) Confocal images of overexpressed MUA-6::mCherry and

SAX-7::GFP. Arrow indicates the region where MUA-6 is overexpressed and arrowhead shows the normal MUA-6 expression region. n=10. Scale bar is 10 μm.

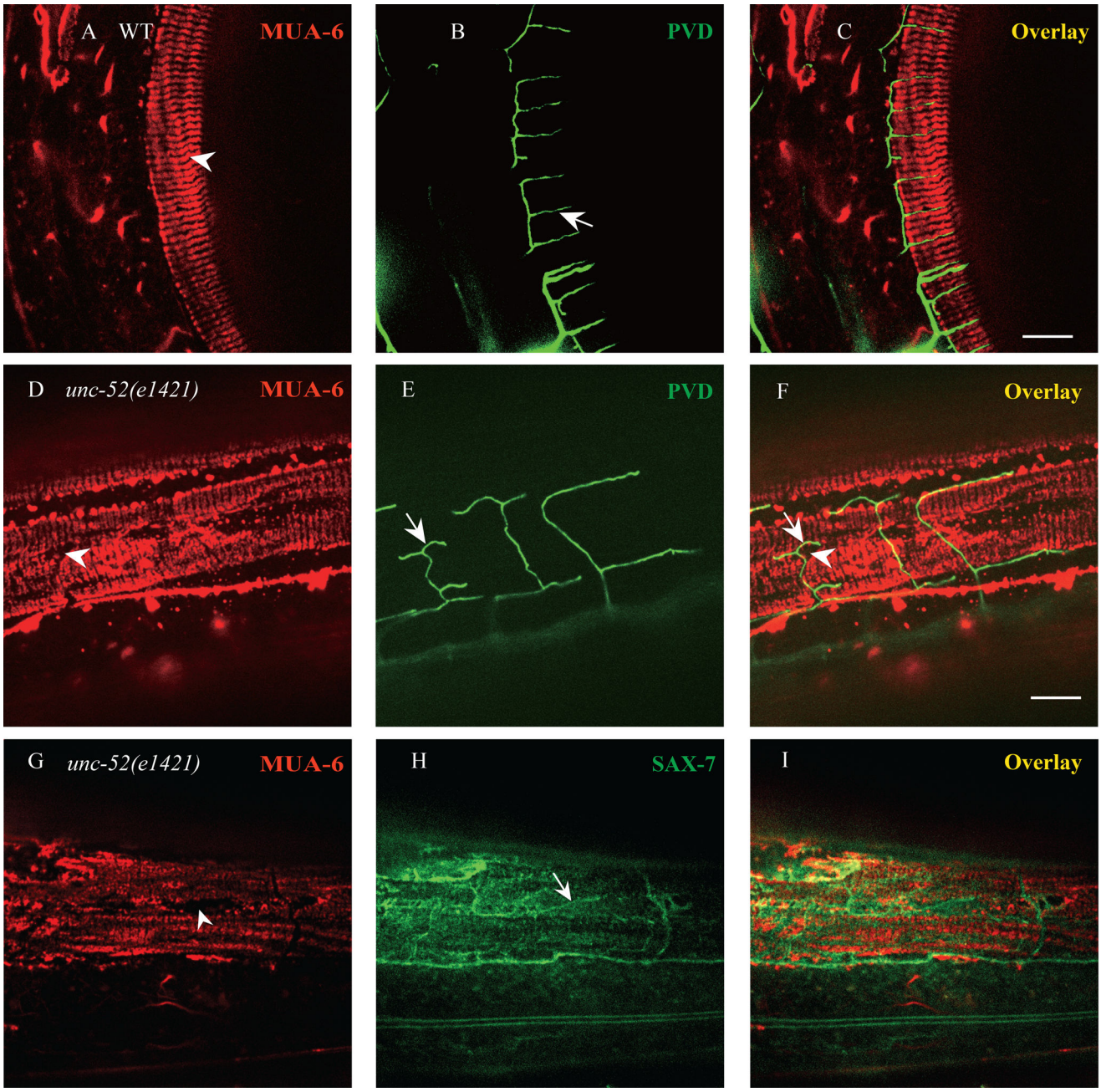

Fig. 7. UNC-52 patterns hypodermal FOs

A–C) Confocal images of MUA-6::mCherry and PVD::GFP in wild type. Arrow indicates PVD quaternary dendrite and arrowhead shows FOs stripe. n=30. D–F) Confocal images of MUA-6::mCherry and PVD::GFP in *unc-52*(*e1421*) mutants. Arrow indicates PVD "T" type quaternary dendrite and arrowhead shows FOs gaps in the stripes. n=30. G–I) Irregular SAX-7 stripes localized to MUA-6 gaps in *unc-52*(*e1421*) mutant. Arrowhead indicates one MUA-6 gap and arrow shows one irregular SAX-7 stripe. n=15. Scale bar is 10 μm.